The Astrophysical Journal, 663:924–932, 2007 July 10

EXPLORING SUPERMASSIVE BLACK HOLE GROWTH WITH ALMA

Nozomu Kawakatu
National Astronomical Observatory of Japan, 2-21-1 Osawa, Mitaka, Tokyo 151-8588, Japan; kawakatu@th.nao.ac.jp

Paola Andreani
European Southern Observatory, Karl Schwarzschild strasse 2, D-85748 Garching, Germany;
INAF-Osservatorio Astronomico di Trieste, via Tiepolo 11, 34131 Trieste, Italy

Gian Luigi Granato
INAF-Ossevatorio Astronomica di Padova, Vicolo dell'Osservatorio 5, I-35100, Padova, Italy;
SISSA/ISAS, via Beirut 2-4, 34014, Trieste, Italy

and

Luigi Danese
SISSA/ISAS, via Beirut 2-4, 34014, Trieste, Italy; INAF-Osservatorio Astronomico di Padova,
Vicolo dell'Ossevatorio 5, I-35100, Padova, Italy
Received 2006 December 18; accepted 2007 March 23

ABSTRACT

Massive tori with $\approx 10^8$–$10^9\ M_\odot$ are predicted to extend on a $\sim$100 pc scale around the center of elliptical galaxy progenitors by a model of a supermassive black hole (SMBH) growth coeval to the spheroidal population of the host galaxy. Direct detection of such massive tori would cast light on a key physical condition that allows the rapid growth of SMBHs and the appearance of QSOs at high redshift. For this reason, we examine the detectability of such structures at substantial redshift with the Atacama Large Millimeter Array (ALMA). We propose that submillimeter galaxies (SMGs) are the best targets to test our predictions. In order to assess the observational feasibility, we estimate the expected number counts of SMGs with massive tori and check the detectability with the ALMA instrument, the unique facility which can resolve the central region of high-redshift objects. Our work shows that ALMA will be able to resolve and detect high-J ($J > 4$) CO emissions from $\sim$100 pc scale extended massive tori up to $z \approx 2$. Observations of lensed SMGs will yield excellent spatial resolution, allowing us to resolve their massive tori at even higher redshift. We further discuss the detectability of the HCN molecule as a better tracer of the high-density gas expected in such tori. The final goal of these kind of observations is to pinpoint possible physical mechanisms for storing very large amounts of gas in the very central galactic regions on timescales of several 10^8 yr.

Subject headings: galaxies: evolution — galaxies: formation — galaxies: nuclei

Online material: color figures

1. INTRODUCTION

The energy emitted by active galactic nuclei (AGNs) is commonly ascribed to accretion onto a supermassive black hole (SMBH). Recent high-resolution observations of galactic centers indicate the presence of a SMBH whose mass correlates with the mass, the velocity dispersion, and the luminosity of the galactic bulge (e.g., Kormendy & Richstone 1995; Richstone et al. 1998; Magorrian et al. 1998; Laor 1998; Ferrarese & Merritt 2000; Tremaine et al. 2002; McLure & Dunlop 2001, 2002; Marconi & Hunt 2003). QSO hosts are mostly luminous and well-evolved early-type galaxies (e.g., McLeod & Rieke 1995b; Bahcall et al. 1997; McLure et al. 2000; Dunlop et al. 2003). Taken together, these observations indicate that the formation of a SMBH, a bulge, and a QSO are closely related to each other. While it is still not clear which is the main mechanism for the formation of a SMBH, many studies suggest that BH growth by gas accretion processes plays an important if not dominant role (Salucci et al. 1999; Fabian & Iwasawa 1999; Yu & Tremaine 2002; Hosokawa 2002; Marconi et al. 2004; Shankar et al. 2004).

Kawakatu et al. (2003, hereafter KUM03) and Granato et al. (2004, hereafter G04) proposed a physical model for the coevolution of QSO BHs and the spheroidal component of galaxies. The formation of the latter is computed with a semianalytical technique, which includes the effects of stellar and QSO feedback, and model outcomes have been more widely compared to observations of several galaxy populations (G04; Silva et al. 2005; Granato et al. 2006; Lapi et al. 2006). In these models, the fueling of the central BH in forming spheroids takes place in two steps: (1) a low angular momentum gas *reservoir* is formed at a rate essentially proportional to the star formation rate on a timescale of a few 10^8 yr; then (2) the reservoir gas is accreted onto the central BH at a rate of the order of the Eddington limit. Since in the earlier phases of SMBH growth the former rate largely exceeds the latter, a massive reservoir accumulates; most of its mass is accreted onto the SMBH only at the last e-folding times ($t_e \simeq 4 \times 10^7$ yr) and powers an enormous energy release, which stops both the star formation and the growth of the reservoir. The massive reservoir is likely to be a geometrically thick massive disk (we call it a massive torus), because of some residual angular momentum. We comment on the passage from the massive reservoir to the massive torus in detail later. A plausible physical mechanism responsible for step (1) is radiation drag (Umemura 2001; Kawakatu & Umemura 2002), and thus we hereafter refer to this as the radiation drag model. However, it should be kept in mind that any other mechanism producing a similar rate of production of massive tori would not alter the essence of these computations.

The scenario proposed by KUM03 and G04 establishes a well-defined sequence connecting various populations of massive spheroidal galaxies: (1) vigorous and rapidly dust-enshrouded

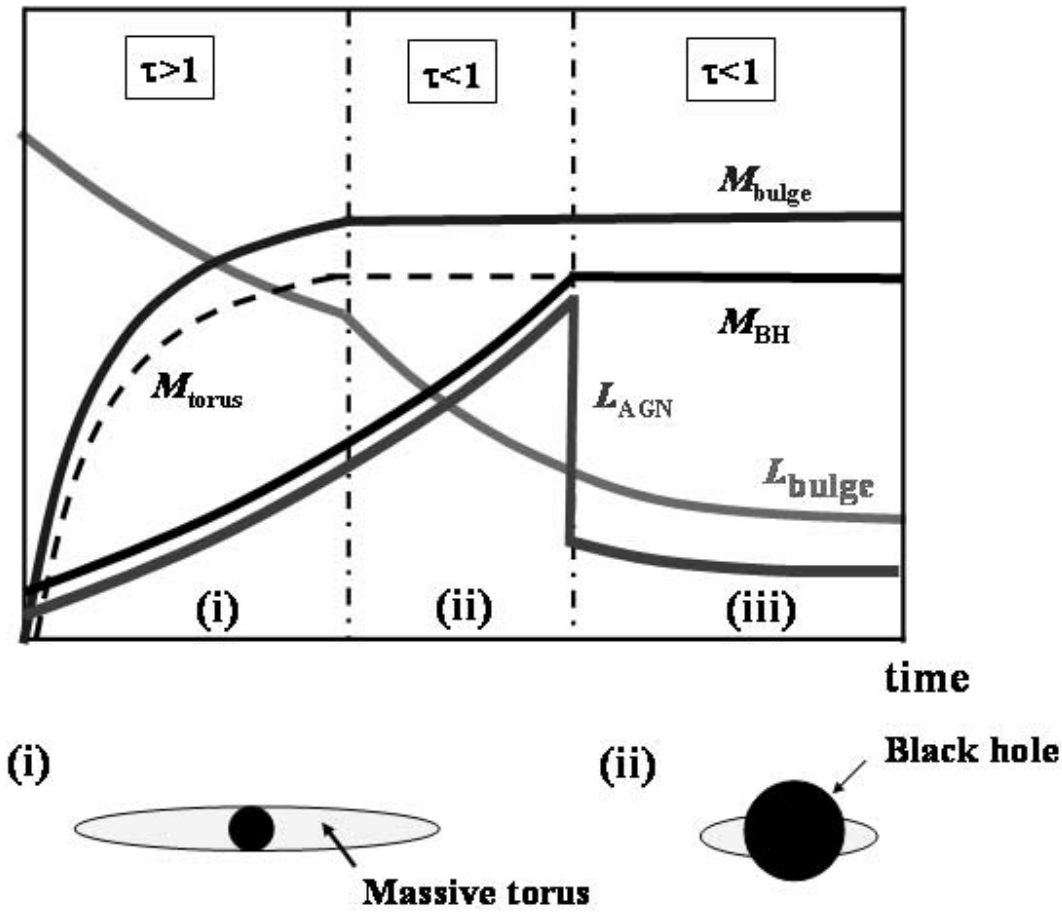

FIG. 1.—Schematic sketch of the coevolution of a SMBH and a galactic bulge. (Adapted with permission from Fig. 1 of Umemura 2001.) The abscissa is time and the ordinate is arbitrary. Here τ is the optical depth of the bulges. Phase (i) denotes the early phase of a QSO (SMG phase). The QSO phase corresponds to the end of phase (ii). In phase (i), a massive torus around a smaller BH is predicted. [*See the electronic edition of the Journal for a color version of this figure*.]

star formation activity, during which a central SMBH grows, explaining the submillimeter galaxy population (SMG), which are examples of high-z ultraluminous infrared galaxies (ULIRGs); (2) a QSO phase, halting subsequent star formation, and (3) an essentially passive evolution of stellar populations, going through an extremely red object (ERO) phase (see Fig. 1; for details, see Figs. 2 and 3 in KUM03 and Fig. 3 in G04).

Here we suggest that the massive torus, before accreting onto the SMBH (the timescale is $\approx 10^8$–10^9 yr), forms a massive torus of the kind envisaged by unified models of AGNs (e.g., Antonucci 1993; Granato & Danese 1994; Urry & Padovani 1995). Thus, the radiation drag model predicts the existence of a massive torus with $\approx 10^8$–$10^9\ M_\odot$ in the early phase of SMBH and spheroid growth (stage [i] and also the beginning of stage [ii]; see Fig. 1). The impact of the direct detection of massive tori is to reveal whether the large mass ratio of a torus to a black hole, $M_{\rm torus}/M_{\rm BH} \gg 1$, is a key physical condition triggering the rapid growth of SMBHs and the appearance of QSOs. This issue will be discussed in detail later. Hence, we investigate the required spatial resolution and expected CO and HCN emission lines from massive tori. We focus our investigation on the high-z universe ($z > 1$) where the peak of QSO activity occurs (around $z \simeq 2$) and where mild AGN activity has already been detected in high-z SMGs (Alexander et al. 2003, 2005a, 2005b), in very good agreement with the G04 predictions (Granato et al. 2006). In particular, we here investigate the detectability of massive tori at $z > 1$ with the next-generation millimeter interferometer, ALMA (Atacama Large Millimeter Array). The rest of this paper is organized as follows. In § 2, we briefly review the formation of massive tori in the early phase of BH growth and set up the model for massive tori. In § 3, we first estimate the expected spatial resolution and expected CO and HCN fluxes from massive tori. Then we discuss the best targets with massive tori and show the number count of candidates with massive tori. Finally, we mention the importance of the velocity mapping on massive tori and the impact on the detection of them for SMBH growth. Our discussions and conclusions are given in § 4. Throughout this paper, we adopt the cosmology indicated by *WMAP* data (Bennett et al. 2003; Spergel et al. 2007), i.e., a flat universe with Hubble parameter $H_0 = 70$ km s^{-1} Mpc^{-1}, $\Omega_M = 0.27$, and $\Omega_\Lambda = 0.73$.

2. MODEL

2.1. *Mass Accretion Due to Radiation Drag*

We review a physical model of the formation of a SMBH in forming spheroids, based on radiation drag-driven mass accretion. The radiation drag, driving the mass accretion, originates in the relativistic effect in absorption and subsequent re-emission of the radiation. This effect is naturally involved in relativistic radiation hydrodynamic equations (Fukue et al. 1997, Umemura

et al. 1997). The angular momentum transfer in radiation hydrodynamics is given by the azimuthal equation of motion in cylindrical coordinates,

$$\frac{1}{r}\frac{d(rv_\phi)}{dt} = \frac{\chi_d}{c}\left[F^\phi - \left(E + P^{\phi\phi}\right)v_\phi\right], \quad (1)$$

where E is the radiation energy density, F^ϕ is the radiation flux, $P^{\phi\phi}$ is the radiation stress tensor, and χ_d is the mass extinction coefficient, which is given by $\chi_d = n_d\sigma_d/\rho_{\rm gas}$, with the number density of dust grains n_d, the dust cross section σ_d, and the gas density $\rho_{\rm gas}$. By solving the radiative transfer, including dust opacity, Kawakatu & Umemura (2002) evaluated the radiative quantities in a clumpy medium, E, F^ϕ, and $P^{\phi\phi}$, and thereby obtained the total angular momentum loss rate. These authors then estimated the total mass of the dusty ISM accreted on to a central massive *reservoir*, $M_{\rm res}$, using the relation $\dot{M}_{\rm gas}/M_{\rm gas} = -\dot{J}/J$, where J and $M_{\rm gas}$ are the total angular momentum and gas of the ISM. Then, the reservoir mass is assessed as

$$M_{\rm res}(t) = \int_0^t \dot{M}_{\rm gas}\,dt = -\int_0^t M_{\rm gas}\frac{\dot{J}}{J}\,dt. \quad (2)$$

In the optically thick regime of radiation drag, $-M_{\rm gas}\dot{J}/J = L_{\rm sph}(t)/c^2$, where $L_{\rm sph}(t)$ is the total luminosity of the spheroids. The radiation-drag efficiency depends on the optical depth τ in proportion to $(1 - e^{-\tau})$ (Umemura 2001). Thus, the total mass of the reservoir can be expressed by

$$M_{\rm res}(t) = \eta_{\rm drag}\int_0^t \frac{L_{\rm sph}(t')}{c^2}\left(1 - e^{-\tau(t')}\right)dt', \quad (3)$$

where $\tau(t)$ is the optical depth of spheroids measured from the center. Here, we estimate the evolution of $\tau(t)$ by using an evolutionary spectral synthesis code PEGASE (Fioc & Rocca-Volmerange 1997). The efficiency $\eta_{\rm drag}$ is found to be maximally 0.34 (Kawakatu & Umemura 2002).

Moreover, it is worth keeping in mind the ratio of reservoir mass to spheroidal mass (see Umemura 2001 for details). The radiation energy emitted by a main-sequence star is 0.14ϵ times the rest-mass energy of the star, m_*c^2, where ϵ is the energy conversion efficiency of nuclear fusion from hydrogen to helium, which is 0.007. Thus, the total luminosity of the spheroids is estimated to be

$$L_{\rm sph}(t) \simeq 0.14\epsilon S_{\rm sph}(t)c^2, \quad (4)$$

where $S_{\rm sph}(t)$ is the star formation rate in the spheroidal system. By substituting this in equation (3), the ratio of reservoir mass to spheroidal mass is given by

$$\frac{M_{\rm res}(t)}{M_{\rm sph}(t)} \simeq 2\times10^{-3}, \quad (5)$$

which is comparable to the observed black hole-to-bulge mass ratio in nearby galaxies. Here $M_{\rm sph} = \int_0^t S_{\rm sph}(t')\,dt'$.

2.2. *Formation of a Massive Torus*

In § 2.1, we introduced the reservoir mass in the context of radiation drag-induced mass accretion. However, the massive reservoir does not evolve into a SMBH directly, because the radiation drag cannot remove the angular momentum thoroughly (Sato et al. 2004). Thus, some residual angular momentum would terminate the radial contraction. In the massive reservoir, the viscosity is expected to work effectively because the viscous timescale is shrunk by the radiation drag (Mineshige et al. 1998). Thus, the massive reservoir is likely to be a massive self-gravitating viscous disk. In such a massive disk, the extreme star formation occurs in the outer part of a massive torus via the gravitational instability, since the Toomre Q parameter is less than unity, where $\kappa c_s/\pi G\Sigma_g$, for the epicycle frequency κ, the sound velocity c_s, and the surface density Σ_g. If this is the case, the massive reservoir will become a *geometrically thick* massive disk (hereafter we call it a massive torus: $M_{\rm torus} = M_{\rm res}$) by supporting the vertical thickness by the energy feedback from supernovae (Wada & Norman 2002) and radiation pressure from the starburst (Ohsuga & Umemura 2001; Thompson et al. 2005; Watabe & Umemura 2005).

As for the BH growth, we here assume that the mass accretion driven by the viscosity onto the BH horizon is determined by an order of the Eddington rate,

$$\dot{M}_{\rm Edd} \equiv L_{\rm Edd}/c^2 \simeq 0.2\ M_\odot\ {\rm yr}^{-1}\ (M_{\rm BH}/10^8\ M_\odot),$$

where $L_{\rm Edd}$ is the Eddington luminosity. As mentioned in § 2.1, the mass accretion rate from a host galaxy to a galactic center via radiation drag is

$$\dot{M}_{\rm drag} \approx L_{\rm sph}/c^2 \simeq 0.1(L_{\rm sph}/10^{12}\ L_\odot)\ M_\odot\ {\rm yr}^{-1}.$$

According to KUM03 (also G04), the starburst phase is closely related to the formation of a QSO. During the first stage, vigorous star formation occurs, while a SMBH is still growing ($M_{\rm BH} \approx 10^6$–$10^7\ M_\odot$). In this phase, the existence of the massive torus with $M_{\rm torus}/M_{\rm BH} \gg 1$ can be predicted, since $\dot{M}_{\rm drag}$ largely exceeds $\dot{M}_{\rm Edd}$. At the end of the starburst phase, the SMBH has grown and radiates at maximum luminosity (QSO phase). In the QSO phase, $M_{\rm BH}$ approaches $M_{\rm torus}$, and thus $M_{\rm torus}/M_{\rm BH} \simeq 1$. After the QSO phase, the AGN luminosity decreases rapidly, since almost all of the matter in the massive torus has fallen onto the central BH; namely, the QSOs would evolve into low-luminosity AGNs (LLAGNs). Hence, $M_{\rm torus}/M_{\rm BH}$ can be expected to be much smaller than unity for spheroidal galaxies with LLAGNs. This is consistent with observations showing that elliptical galaxies and galactic bulges have no gas. It can therefore be concluded that the evolution of the mass ratio ($M_{\rm torus}/M_{\rm BH}$) reflects the history of SMBH growth.

2.3. *Physical Parameters of Massive Tori*

The radiation drag mechanism, as mentioned in §§ 2.1 and 2.2, predicts the presence of massive tori with masses $M_{\rm torus} \simeq 10^8$–$10^9\ M_\odot$, equal to the final masses of BHs powering QSOs (see Fig. 1). Typical length scales of such tori can be expressed by the accretion radius of the "BH plus massive torus" system (r_a). The accretion radius is given by $r_a = G(M_{\rm BH} + M_{\rm torus})/\sigma_{\rm sph}^2$, where $\sigma_{\rm sph}$ is the velocity dispersion of the spheroids. Following the virial theorem for spheroids ($\sigma_{\rm sph}^2 = GM_{\rm sph}/r_b$), the radius can be written as

$$r_a = \left(\frac{M_{\rm BH} + M_{\rm torus}}{M_{\rm sph}}\right)r_b \simeq \left(\frac{M_{\rm torus}}{M_{\rm sph}}\right)r_b, \quad (6)$$

where r_b is the effective radius of the spheroids. Here we consider the case of $M_{\rm BH} \ll M_{\rm torus}$, since we focus on the rapid growth phase (see stage [i] in Fig. 1). By substituting equation (5) in equation (6), the r_a can be estimated by $r_a \simeq 20$ pc (r_b/10 kpc). In the present paper, the size of a massive torus is defined as $r_{\rm torus} = Ar_a$. The factor A can be inferred from high-resolution observations of tori in nearby AGNs (e.g., Jaffe et al. 1993;

van der Marel et al. 1998; Davies et al. 2006) and turns out to be at least $A \approx 5$. Recent IR and X-ray observations suggest that these are $\sim$100 pc scale extended massive tori (e.g., McLeod & Rieke 1995a; Maiolino et al. 1995; Maiolino & Rieke 1995; Granato et al. 1997; Malkan et al. 1998) rather than compact massive tori. However, $r_{\rm torus}$ (or A) is physically determined by the quantity of residual angular momentum removed by the radiation-drag process. In order to understand this issue, we need to explore sophisticated numerical simulations, which will be the subject of our future studies. Thus, a compact massive torus cannot be ruled out physically. In this paper, we examine two cases: one is a compact torus with $r_{\rm torus} = 20$ pc ($A = 1$), the other is an extended torus with $r_{\rm torus} = 100$ pc ($A = 5$).

Concerning the rotation law and the surface density profile in massive tori, we assume $v_\phi(r) = v_{\phi,0}(r/r_{\rm torus})^{-\alpha}$ and $\Sigma_g(r) = \Sigma_{g,0}(r/r_{\rm torus})^{-\beta}$, where $v_{\phi,0}$ and $\Sigma_{g,0}$ are the quantities at $r_{\rm torus}$. Here $\Sigma_{g,0}$ is related to the torus mass through $M_{\rm torus} = \int_{r_{\rm in}}^{r_{\rm torus}} 2\pi r \Sigma_g(r)\, dr$, where $r_{\rm in}$ is the sublimation radius for graphite grains. The size $r_{\rm in}$ is expressed as $r_{\rm in} = 1.3 L_{\rm UV,46}^{0.5} T_{1500}^{-2.8}$ pc, where $L_{\rm UV,46}$ is the AGN UV luminosity in units of 10^{46} erg s^{-1}, and T_{1500} is the grain sublimation temperature in units of 1500 K (Barvainis 1987). Recently, Suganuma et al. (2006) measured the inner edge of a dusty torus, $r_{\rm in}$, by the reverberation mapping technique, and their observational results strongly suggest that $r_{\rm in}$ is determined by the dust sublimation radius. Although the size $r_{\rm in}$ depends on the size of dust grains and dust composition (e.g., Laor & Draine 1993), this does not significantly affect the expected line flux for $r_{\rm in} \ll r_{\rm torus}$. Thus, we set $r_{\rm in} = 1$ pc in the present paper. The rotation velocity, $v_{\phi,0} = A^{-\alpha} v_\phi(r_a)$, can be determined from $v_\phi(r_a) = \sigma_{\rm sph}$. Since α and β are unknown free parameters, we calculate the CO flux density corresponding to the following parameter set: $\alpha = -1$, 0, and 0.5 and $\beta = 0$, 1, and 2.

Provided that the scale heights ($h_{\rm torus}$) of massive tori are $\sim 0.3 r_{\rm torus}$ (e.g., Wada & Norman 2002), the average number density and column density of molecular hydrogen are

$$n(\mathrm{H_2}) \approx 10^3\ \mathrm{cm^{-3}}\ \left(M_{\rm gas}/10^8\ M_\odot\right)\left(r_{\rm torus}/100\ \mathrm{pc}\right)^{-3}$$

and

$$N(\mathrm{H_2}) \approx 10^{23}\ \mathrm{cm^{-2}}\ \left(M_{\rm gas}/10^8\ M_\odot\right)\left(r_{\rm torus}/100\ \mathrm{pc}\right)^{-2},$$

respectively. Thus, massive tori are optically thick and thermalized at CO lines. This holds for any molecular cloud with a hydrogen column density larger than $N(\mathrm{H_2}) > 10^{21}$ cm^{-2} (e.g., Tielens & Hollenbach 1985). For $h_{\rm torus}$, we expect the opening angle to be almost zero in the quite extreme conditions we are envisaging. However, the expected CO flux density does not depend on $h_{\rm torus}$, as long as the massive tori are optically thick for CO lines.

Ohsuga & Umemura (2001) analyzed the gas temperature, $T_{\rm gas}$, of the optically thick massive torus by using one-dimensional radiation hydrodynamic equations, coupled with ionization and thermal processes. They found that dust cooling is effective, and the gas temperature $T_{\rm gas}$ is thus $\approx$100 K. We therefore assume $T_{\rm gas} = 100$ K in this paper. This is also supported by the recent numerical results suggesting that massive tori would be dominated by cold ($T_{\rm gas} \sim 100$ K) and dense [$n(\mathrm{H_2}) \approx 10^2$ cm^{-3}] molecular gas (e.g., Wada & Tomisaka 2005). Finally, we note that the CO luminosity and the CO-to-H_2 conversion factor are a function of the metallicity (Radford et al. 1991) and that the far-UV flux from AGNs and/or massive stars is lower by a few magnitudes for $n(\mathrm{H_2}) > 10^2$ cm^{-3} (e.g., Tielens & Hollenbach 1985; Mochizuki & Nakagawa 2000).

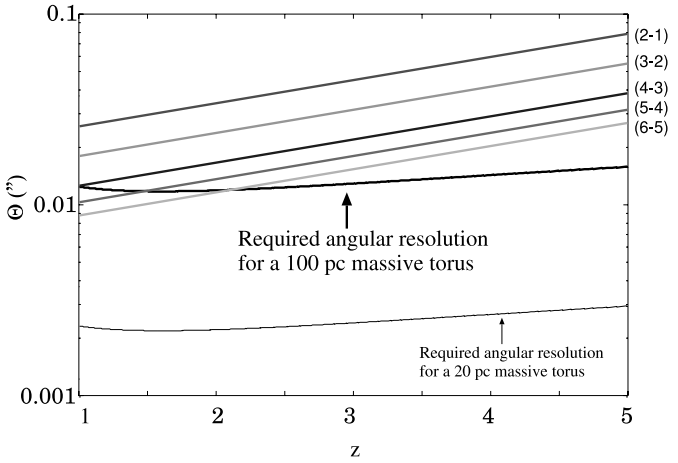

FIG. 2.—Required spatial resolution (arcsec) for a 20 pc scale (*thin horizontal line*) and a 100 pc scale (*thick horizontal line*) massive torus against redshift z. The five lines represent the possible spatial resolution for CO lines in the transition level ($J, J-1$) with the ALMA instrument. [*See the electronic edition of the Journal for a color version of this figure.*]

3. RESULTS

3.1. *Required Spatial Resolution*

Figure 2 shows the spatial resolution required to detect 100 pc scale extended massive tori. A resolution of $\approx 0.01''$ is necessary, well beyond the capabilities of present-day millimeter and submillimeter interferometers (typically $\approx 0.5''$). Conversely, the angular resolution of ALMA from 86–720 GHz with $\Theta('') \simeq 0.005('')(\nu_{\rm obs}/600\ \mathrm{GHz})^{-1}$ is sufficient to resolve high-J ($J > 4$) molecular emissions from 100 pc scale extended massive tori, where $\nu_{\rm obs}$ is the observed frequency.[1] On the other hand, 20 pc scale compact massive tori cannot be resolved unless the objects are gravitationally lensed (e.g., Downes & Solomon 2003). The lensing effect magnifies not only the intrinsic CO line luminosity, but also the scale of the emitting region. If we assume that the magnified CO image is an ellipse, the magnification factor is $\mu = a/r_{\rm torus}$, where $a = D_A \Theta_{\rm obs}/2$ is the apparent semimajor axis of the magnified image, and D_A and $\Theta_{\rm obs}$ are the angular distance and the observed angular length of the magnified image, respectively. Thus, it is possible to achieve super-resolution, which can be μ times as high as the instrumental resolution, e.g., $\mu = 2$–50 for lensed SMGs (Solomon & Vanden Bout 2005). As seen in Figure 2, for lensed objects, we can resolve lower J CO lines from massive tori and/or study massive tori at higher redshift.

3.2. *Expected Flux of the* CO *Molecule*

Since most molecular clouds in massive tori are cold and dense (§ 2), it is expected that CO molecular lines are good tracers of molecular gas mass. In this paper, we express the CO line luminosity $l'_{\rm CO}(J, J-1)$ in units of K km s^{-1} as the product of the velocity-integrated source brightness temperature $T_b \Delta v_{\rm rest}$, where $\Delta v_{\rm rest}$ is the rest-frame line width. Then the CO line luminosity in the arbitrary transitional level from J to $J-1$ is given by $l'_{\rm CO}(J, J-1) = T_b \Delta v_{\rm rest}$. Thus, the CO line luminosity ratio for two lines, $R_{J,J-1} = l'_{\rm CO}(J, J-1)/l'_{\rm CO}(1, 0)$, in the same source is equal to the ratio of the intrinsic brightness temperature. Since we deal with CO lines that are optically thick and thermalized up

[1] This comes from the ALMA Web site (http://www.eso.org/projects/alma/science/bin/sensitivity.html). See note 3 in this Web site.

TABLE 1
VALUES OF THE FUNCTION $H(\alpha, \beta)$

α	$\beta = 0$	$\beta = 1$	$\beta = 2$
−1	2	1	20 (7)
0	1	1	1
0.5	0.8	0.7[a]	0.4 (2)

NOTES.—The values in parenthesis are for 20 pc compact massive tori. The others correspond to the case of 100 pc extended massive tori.
[a] The fiducial case in this paper.

to $J = 6$, we set $R_{J,J-1} = 1$. Note that the gas temperature can be warmer than in normal galaxies due to both the intense radiation field via the huge star-forming activity and the accretion onto their central growing BH. A flat distribution of Rayleigh-Jeans brightness temperature up to $J = 6$ has been reported in starburst galaxies (e.g., Kawabe et al. 1999).

The line flux density $f_{\rm CO}(J, J-1)$ in units of Jy pc^{-2} corresponding to the CO line luminosity $l'_{\rm CO}(J, J-1)$ can be derived. Using the H_2 mass-to-CO line luminosity relation $l'_{\rm CO}(J, J-1)(r) = R_{J,J-1}\Sigma({\rm H_2})(r)/X_{\rm CO}$, the corresponding received CO flux density $f_{\rm CO}(J, J-1)$ is

$$f_{\rm CO}\,(J, J-1)(r) = \frac{2\kappa}{c^2}\frac{l'_{\rm CO}(J, J-1)(r)\nu^2_{\rm rest}(J, J-1)(1+z)}{\Delta v_{\rm rest}(r)}\frac{\cos(i)}{D_L^2}, \quad (7)$$

where κ is the Boltzman constant, i is the inclination angle of the massive torus, $f_{\rm CO}(J, J-1)$ is the observed flux density in Jy pc^{-2}, $\Sigma({\rm H_2})(r) = \Sigma_g(r)$, $\Delta v_{\rm rest}(r) = v_\phi(r)$, $\nu_{\rm rest}(J, J-1) = 115J$ GHz is the rest frequency of the transition, and D_L is the luminosity distance. Here $X_{\rm CO} = 0.8\ M_\odot\ ({\rm K\ km\ s^{-1}})^{-1}$ is a typical value adopted for ULIRGs and SMGs (Downes & Solomon 1998; Solomon & Vanden Bout 2005). This value is comparable to $X_{\rm CO} \simeq 0.5\ M_\odot\ ({\rm K\ km\ s^{-1}})^{-1}$, which was calculated by three-dimensional, non–local thermal equilibrium radiative transfer calculations for high-J CO lines (e.g., $J = 3$ and $J = 4$) emitted from inhomogeneous dusty tori (Wada & Tomisaka 2005).

The integrated CO flux density (Jy) of massive tori over their surface can be calculated by $S_{\rm CO}(J, J-1) = \int_{r_{\rm in}}^{r_{\rm torus}} 2\pi r f_{\rm CO}(J, J-1)(r)\,dr$. Then

$$S_{\rm CO}(J, J-1) \approx 10^3\ {\rm Jy}\ J^2 H(\alpha = 0.5, \beta = 1)\left(\frac{X_{\rm CO}}{0.8}\right)^{-1} \times \left(\frac{R_{J,J-1}}{1.0}\right)\left(\frac{M_{\rm torus}}{3\times10^8\ M_\odot}\right)\left(\frac{\Delta v_{\rm rest,0}}{100\ {\rm km\ s^{-1}}}\right)^{-1}\frac{1+z}{D_L^2}, \quad (8)$$

where

$$\Delta v_{\rm rest,0} = 100\ {\rm km\ s^{-1}}\left(\frac{A}{5}\right)^{-(\alpha/0.5)} \times \left(\frac{M_{\rm torus}}{3\times10^8\ M_\odot}\right)^{0.5}\left(\frac{r_a}{20\ {\rm pc}}\right)^{-0.5},$$

with an inclination angle equal to 45°, and $H(\alpha, \beta)$ is a function of α and β. We summarize the values of $H(\alpha, \beta)$ in Table 1.

Figure 3 shows the expected CO emission from 100 pc scale extended massive tori as a function of redshift for a fiducial case ($M_{\rm torus} = 3\times10^8\ M_\odot, A = 5, \alpha = 0.5$, and $\beta = 1$). The five lines denote the CO flux density $S_{\rm CO}(J, J-1)$ at the transition level $(J, J-1)$. To the left of the filled circles, each line can be resolved with ALMA (see Fig. 1). The CO lines without filled circles cannot be resolved. The horizontal line shows the ALMA detection limit (50 antennas) at 0.5 mJy (5 σ requested data) in the 25 km s^{-1} channel over 12 hr of on-source integration time.[2] The high-J CO lines ($J > 4$) can be detected and resolved up to $z = 2$ with ALMA. Again, it is worth recalling that for gravitationally lensed objects, we can detect lower J-CO lines and/or study higher redshift objects, because the observed CO flux density increases μ times with respect to that estimated in equation (8).

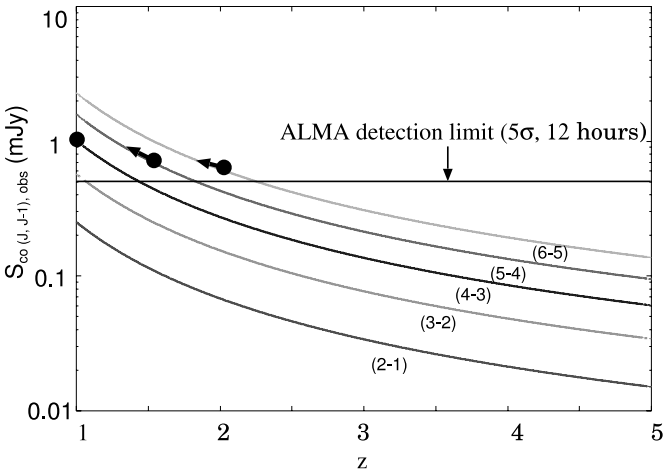

FIG. 3.—Expected CO emission (mJy) from massive tori against redshift z in the fiducial case ($M_{\rm torus} = 3\times10^8\ M_\odot$, $A = 5$, $\alpha = 0.5$, and $\beta = 1$). The five lines denote the CO flux density $S_{\rm CO}(J, J-1)_{\rm obs}$ at the transition level $(J, J-1)$ at the rest frame. The horizontal line represents the ALMA detection limit (50 antennas) at 0.5 mJy (5 σ requested data) in the 25 km s^{-1} channel over 12 hr of on-source integration time. To the left of the filled circles, each line can be resolved spatially. [*See the electronic edition of the Journal for a color version of this figure.*]

Finally, we discuss the dependence of A (or $r_{\rm torus}$), α, and β on $S_{\rm CO}(J, J-1)$. First, we investigate the effect of the function $H(\alpha, \beta)$. As seen in Table 1, it is found that $H(\alpha, \beta)$ is of order unity, except for the case of $\alpha = -1$ and $\beta = 2$. In this case, the expected CO flux density $S_{\rm CO}(J, J-1)$ has a larger value than in the other cases, because of high gas concentrations and slower rotation velocities in the inner regions of massive tori. As mentioned in § 2.3, $\Delta v_{\rm rest,0}$ is linked to the size of the torus. Thus, the emissivity $S_{\rm CO}(J, J-1)$ also depends on the value of $r_{\rm torus}$ (or A). Then, the CO flux density of compact massive tori ($A = 1$, $\alpha = 0.5$, and $0 \le \beta < 2$) is ~3 times as small as the fiducial case, because the $\Delta v_{\rm rest,0}$ of compact massive tori is larger than that in the fiducial case. Thus, the detection of compact massive tori with ALMA would be more difficult than the detection of extended massive tori, taking into account the spatial resolution (§ 3.1). Third, the variation of α also affects $S_{\rm CO}(J, J-1)$ for extended massive tori ($A = 5$ and $0 \le \beta < 2$). From equation (8), the $S_{\rm CO}(J, J-1)$ of extended massive tori with rigid rotation ($\alpha = -1$) and flat rotation ($\alpha = 0$) are about 0.1 and 0.5 times smaller that in the fiducial case, respectively. From this we find that it will be difficult to detect the extended massive tori with ALMA if they rotate rigidly. To summarize the results of §§ 3.1 and 3.2, we conclude that 100 pc extended massive tori can be

[2] Note that the ALMA detection limit for lines depends on the observed bands as follows: 0.31 mJy for band 3 (86–116 GHz), 0.42 mJy for band 4 (125–163 GHz), 0.39 mJy for band 5 (163–211 GHz), 0.46 mJy for band 6 (211–275 GHz), and 0.50 mJy for band 7 (275–370 GHz), which can be obtained by the ALMA sensitivity calculator, as mentioned on the ALMA Web site (http://www.eso.org/projects/alma/science/bin/sensitivity.html). Here we take the greatest value (0.50 mJy).

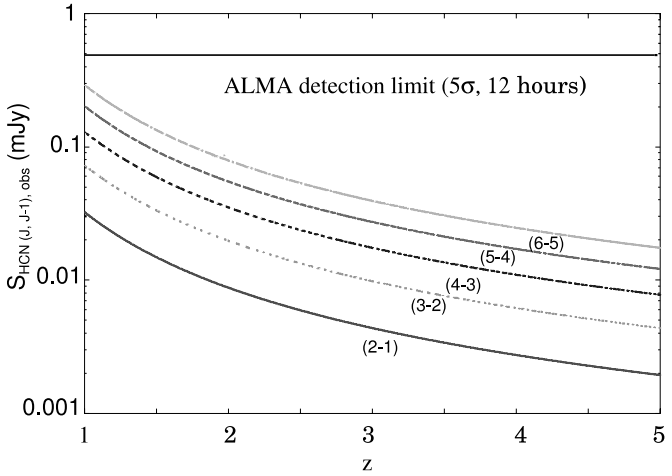

FIG. 4.— Expected HCN emission (mJy) from massive tori against redshift z in the fiducial case ($M_{\rm torus} = 3 \times 10^8\ M_\odot$, $A = 5$, $\alpha = 0.5$, and $\beta = 1$). The lines are the same as in Fig. 3. [*See the electronic edition of the Journal for a color version of this figure*.]

resolved and detected with ALMA, except for extended rigid rotating massive tori.

3.3. *Expected Flux of the* HCN *Molecule*

HCN emission was observed locally in giant molecular clouds and in nearby galaxies (see, e.g., Gao & Salomon 2004 and references therein). At high redshifts, only gravitationally lensed sources have been detected, namely H1413+117 (Cloverleaf) at $z = 2.6$, IRAS F10214+4724 at $z = 2.3$, and the quasar APM 08279+5255 at $z = 3.911$ (Solomon et al. 2003; Vanden Bout et al. 2004; Wagg et al. 2005).

To estimate the flux of the high-z targets discussed here, we assume that the HCN molecule has the same velocity width of the CO line, since both emissions originate within the same dynamical structure (Wagg et al. 2005). As observed for CO lines, we suppose that HCN luminosity is proportional to molecular hydrogen mass. For normal galaxies, a relation between CO and HCN luminosities is established (Gao & Solomon 2004), typically $l'_{\rm HCN}/l'_{\rm CO} \approx 0.1$. For most ULIRGs with AGNs, this ratio turns to be higher, >0.2 (Imanishi et al. 2006). Here we take the value of 0.2, similar to that of Mrk 231 and IRAS 17208−0014, and not far from that of APM 08279+5255 (0.34). The HCN line flux is then $l'_{\rm HCN}(1,0) = 0.3(X_{\rm HCN}/3.3)^{-1}(X_{\rm CO}/0.8)^{-1}\Sigma_g$, which is similar to the relation $l'_{\rm HCN}(1,0) = \Sigma_g/X_{\rm HCN}$, where $X_{\rm HCN} \sim 7\ M_\odot$(K km s^{-1}) for warm gas (Wagg et al. 2005).

In Figure 4, we compare the expected HCN line emission from 100 pc scale extended massive tori ($M_{\rm BH} = 3 \times 10^8\ M_\odot$, $A = 5$, $\alpha = 0.5$, and $\beta = 1$) as a function of redshift to the ALMA sensitivity limit. The dependences of A (or $r_{\rm torus}$), α, and β are same as in the case of CO lines (§ 3.2). The detection of HCN lines from massive tori is more difficult because of the lower abundance of this molecule with respect to CO. At $z \approx 1$, the detection of the central massive torus in this line would require more than 24 hr of on-source integration in the highest angular resolution configuration. In lower resolution configurations, this line is detected at any redshift; however, the constraint presented in this model will not be stringent. It will be possible to detect and resolve HCN lines for gravitationally lensed objects.

3.4. *Which Objects are Associated with Massive Tori?*

We discuss here the best targets associated with massive tori and their expected number counts. Observationally, the majority of SMGs are coeval with QSO activities at $z \approx 2$. From their properties (the massive dynamical mass, the high star formation rate, etc.), SMGs are considered to be progenitors of present-day elliptical galaxies (e.g., Smail et al. 2004). Recent ultradeep X-ray observations have suggested that >50% of SMGs have AGNs whose luminosities are relatively lower than those of coeval QSOs (Alexander et al. 2005b). Thus, following our reference model, we expect massive tori to already be in place in these galaxies and to be feeding the growth of the central BH with $M_{\rm BH} \approx 10^6$–$10^7\ M_\odot$ (Borys et al. 2005). Recently, Menéndez-Delmestre et al. (2007) and Valiante et al. (2007) observed the mid-infrared spectra of a sample of SMGs, finding that in the rest-frame ∼6–8 μm there is a contribution from a relatively weak AGN continuum emission to be added to the contribution from star formation (see Fig. 3 in Valiante et al. 2007). Thus, their results stress once again that the most interesting targets in the search for tori could be the submillimeter galaxies with 24 μm counterparts. According to KUM03 (also G04), the dust emission from massive tori in SMGs is cooler than that in QSOs because of the higher column density of massive tori and the relatively weaker AGN activity. It will also be worth comparing the rest-frame infrared color [e.g., $f(25\ \mu{\rm m})/f(60\ \mu{\rm m})$] of SMGs with that of coeval QSOs. Moreover, Greve et al. (2005), Tacconi et al. (2006), and Gao et al. (2007) have reported ∼10 CO detected SMGs and ∼5 HCN detected SMGs, indicating the presence of large masses of dense gas ($\approx 10^{10}\ M_\odot$) within ∼4 kpc. SMGs are largely present among the early universe molecular emission line galaxies (EMGs) listed by Solomon & Vanden Bout (2005); a significant fraction are also lensed objects.

Therefore, SMGs (especially SMGs with AGNs) are good candidates for exploring massive tori and testing the radiation-drag model. We evaluate the expected number count of SMGs with massive tori with the G04 model. Note that the G04 model predicts number counts, redshift distribution, and AGN accretion rates of SMGs in very good agreement with observations (G04; Silva et al. 2005; Granato et al. 2006). Figure 5 shows the redshift distributions of bright SMGs with different masses of massive tori. The expected number count of galaxies with $M_{\rm torus} > 10^8\ M_\odot$ is ∼100–200 deg^{-2} at $1 < z < 3$. By comparing our predictions with the ALMA data, it would be possible to test and refine the radiation-drag model.

Finally, scaled down versions of star-forming galaxies harboring AGNs can be studied in the local universe. The narrow-line Seyfert galaxies (NLS1s) and ULIRG (especially type I ULIRGs) are characterized by a smaller BH and a higher mass accretion rate (e.g., Pounds et al. 1995; Boller et al. 1996; Mineshige et al. 2000; Mathur et al. 2000; Collin & Kawaguchi 2004; Hao et al. 2005; Kawakatu et al. 2006, 2007). Thus, they would correspond to the early phase of BH growth. If massive tori are detected in targets at $z < 0.01$, they will be easily resolved with present millimeter interferometers as well. Indeed, CO emissions from <100 pc have already been detected in the nearby NLS1 NGC 4051 (L. Tacconi 2005, private communication). By investigating the existences of massive tori in SMGs (spheroids), ULIRGs (spheroids and disk galaxies), and NLS1s (disk galaxies), it will be possible to clarify whether the BH growth process depends on the morphology of host galaxies and redshift.

3.5. *Velocity Mapping of Massive Tori*

For low-z targets, ALMA can study not only the existence of massive tori, but also the subparsec structures of massive tori, although it is difficult for high-z objects. We thus make the channel maps of molecular lines with ALMA, as did Davies et al. (2006) for the nearby Seyfert galaxy NGC 3227. It is consequently possible to distinguish between the circular velocity v_ϕ and the

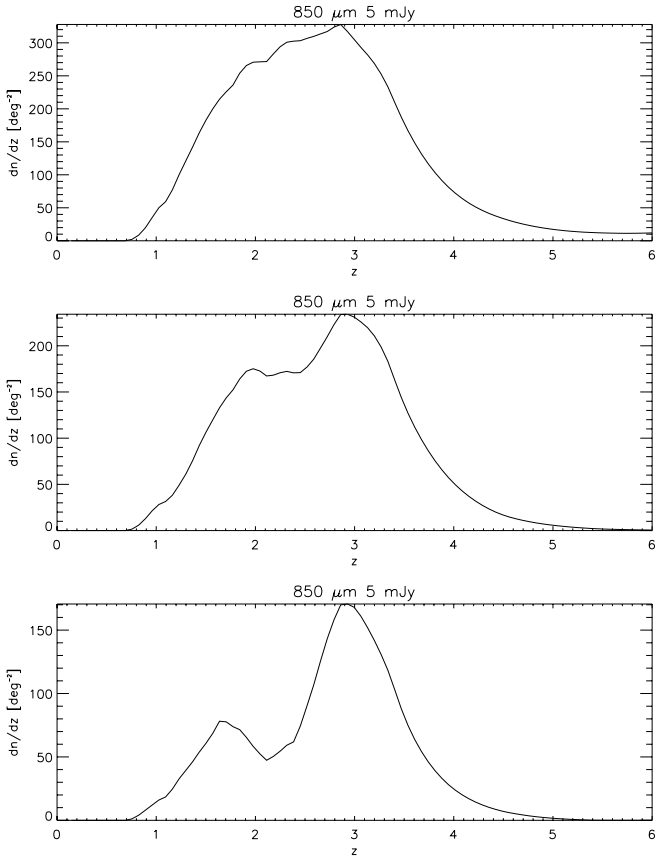

FIG. 5.—Number counts of SMGs with massive tori, dn/dz (deg^{-2}), against redshit z. Top panel shows the number counts of all SMGs. The middle panel denotes dn/dz (deg^{-2}), with $M_{\rm torus} > 10^8\ M_\odot$. The bottom panel shows the number counts of galaxies with massive tori $M_{\rm torus} > 3 \times 10^8\ M_\odot$.

velocity dispersion σ in the region above the spatial resolution of ALMA, that is, from a few pc to $\sim$100 pc (e.g., Fig. 3 in Wada & Tomisaka 2005). If σ is comparable to v_ϕ in massive tori, it means that the kinetic energy is dominated by the random motion. In order to maintain the vertical structure, the continuous energy injection should be necessary, because the cooling time of molecular clouds via collisions is comparable to the orbital period. As mentioned in § 2.2, the radiation pressure via starburst and/or the internal turbulence caused by supernova explosions may be a plausible origin of its energy source. If the scale height of the torus is determined by a balance between the vertical components of the centrifugal force due to a central SMBH and the vertical velocity dispersion (e.g., Wada & Norman 2002), the ratio σ/v_ϕ reflects the ratio $h_{\rm torus}/r_{\rm torus}$, where $h_{\rm torus}$ is the scale height in the body of the massive torus. Hence, the velocity mapping of massive tori is helpful in providing a quantitative estimate of the origin of geometrically thick obscuring tori.

In addition, we expect the starburst luminosity in a massive torus to be closely related to its vertical structure, and the determination of this through ALMA observations is a fundamental test of this model. ALMA velocity mapping assesses the velocity dispersion σ and the scale height $h_{\rm torus}$ for low-z massive tori, and thus it allows us to estimate the viscous coefficient of turbulent motion $\nu_{\rm turb} \sim \sigma h_{\rm torus}$, assuming the largest eddy size is comparable to $h_{\rm torus}$. Using $\nu_{\rm turb}$, we can estimate the mass accretion rate due to the turbulent viscosity, $\dot{M}_{\rm BH} \sim M_{\rm torus}/t_{\rm vis}$, where $t_{\rm vis} \sim r^2/\nu_{\rm turb}$. Thus, we will be able to check whether the mass accretion rate via the turbulent viscosity is a key element in explaining the AGN activity, because both $M_{\rm torus}$ and $\nu_{\rm turb}$ are observable. In order to get an insight into the physics of the fueling process, it would be valuable to derive the radial velocity $v_r(r)$, which would depend on the mass accretion process (e.g., the gravitational torque from a nonaxisymmetric potential, the turbulent viscosity, the radiation avalanche, etc.). Therefore, the velocity mapping of massive tori is essential to exploring the formation of obscuring massive tori and also the fueling process from $\sim$100 pc to $\sim$1 pc, which is a well known "missing link" in the AGN fueling problem.

3.6. *Impact of the Detection of Massive Tori on SMBH Growth*

In § 3.2, we showed that 100 pc scale extended massive tori can be resolved and detected with ALMA. Here, we discuss how the detection of massive tori helps in exploring SMBH growth. A plausible theoretical process of mass accretion onto a central BH is the turbulent viscous drag whose timescale is $t_{\rm vis} \sim r^2/\nu_{\rm turb}$. We adopt $\nu_{\rm turb} = R_{\rm crit}^{-1} r v_\phi$, where $R_{\rm crit} = 100$–1000 and v_ϕ are the critical Reynolds numbers for the onset of turbulence (e.g., Duschl et al. 2000; Burkert & Silk 2001) and the rotation velocity, respectively. The viscous time is given by $t_{\rm vis} = R_{\rm crit} t_{\rm dyn}$, where the dynamical timescale is determined by the central BH plus a surrounding massive torus system. As a result, the mass accretion rate ($\dot{M}_{\rm BH}$) via the viscous drag is given as $\dot{M}_{\rm BH} \propto (M_{\rm torus}/M_{\rm BH})^{3/2}[1 + (M_{\rm BH}/M_{\rm torus})]^{-1/2}$ (see also eq. [22] in Granato et al. 2004). If massive tori with $M_{\rm torus}/M_{\rm BH} \gg 1$ in SMGs are detected with ALMA, the high mass accretion rate (close to the Eddington or super-Eddington accretion rate) would be a common feature of SMGs (especially hard X-ray detected SMGs). This statement can be checked by comparing the X-ray properties (steep photon index, rapid variability, etc.) with those seen in NLS1s in future X-ray missions.

Moreover, KUM03 (also G04) predict that the mass ratio $M_{\rm torus}/M_{\rm BH}$ can be $\sim$1 in the QSO phase, because the growth of QSO BHs has almost finished and/or we are seeing the final e-folding time (see Fig. 1). It would then be worth comparing the massive tori in QSOs with those expected in SMGs with $M_{\rm torus}/M_{\rm BH} \gg 1$. Thus, this parameter ($M_{\rm torus}/M_{\rm BH} \gg 1$) is a key physical condition for the rapid growth of SMBHs and the appearance of QSOs, and its evolution tailors the history of the BH growth process. Considering that the mass of a 100 pc scale dusty torus is much smaller than the central SMBH mass for nearby spheroidal galaxies (e.g., Djorgovski et al. 1991 and Tadhunter et al. 2003 for Cygnus A; Jaffe et al. 1993 and Ferrarese et al. 1996 for NGC 4261; van der Marel et al. 1998 for NGC 7052), it would be a natural interpretation that the large amount of gas around central BHs in SMGs accretes until exhaustion to grow to a SMBH with $\approx 10^8$–$10^9\ M_\odot$ on a timescale of several 10^8 yr. Therefore, the detection of massive tori in SMGs would imply that the SMBH grows from $\approx 10^6$ to $\approx 10^9\ M_\odot$ mainly via the gas accretion process, not through the merger of compact objects.

Finally, we should comment on the case in which ALMA detects less massive tori in SMGs than what we expect, i.e., $M_{\rm torus}/M_{\rm BH} \leq 1$. If this is the case, it might indicate that the growth rate of central BHs in SMGs is much faster than the mass accretion rate from a host galaxy to a massive torus or that some SMGs do not have the potential to evolve into QSOs with $M_{\rm BH} \approx 10^8$–$10^9\ M_\odot$. Whether or not this is the case, we suggest that exploring massive tori would cast light on the SMBH growth process and formation scenario of QSOs.

4. DISCUSSION AND CONCLUSIONS

Given the sensitivity and angular resolution of ALMA, detailed mapping of the CO emissions of galaxies at $z \sim 2$ will

resolve structures on linear scales of $\sim$100 pc and with masses $M_{\rm torus} \approx 10^8$–$10^9\ M_\odot$, the expected size of massive tori around SMBHs. These capabilities can therefore be used in order to explore SMBH growth in SMGs, which are protospheroidal galaxies undergoing huge star formation, just before the onset of the peak of the QSO activity in their center. The results of Alexander et al. (2003, 2005a, 2005b) show that nuclear X-ray luminosity $L_{\rm X} \geq 3 \times 10^{43}$ erg s^{-1} is often associated with SMGs, witnessing a stage in which the SMBHs have masses $M_{\rm BH} \sim 10^6$–$10^7\ M_\odot$ (Borys et al. 2005). If we can detect massive tori with ALMA within the same population, we can definitely conclude that $M_{\rm torus}/M_{\rm BH} \gg 1$ is the key physical condition for the rapid growth of SMBHs and the appearance of QSOs. Moreover, the existence of massive tori in SMGs would imply that the SMBH grows from $\approx 10^6$ to $\approx 10^9\ M_\odot$ via the gas accretion process rather than the merger of compact objects.

In order to assess the observational feasibility, we estimate the expected number counts of SMGs with massive tori and check the detectability with the ALMA instrument. ALMA will be able to resolve and detect high-J CO emissions ($J > 4$) from massive tori up to $z \approx 2$ at the 5 σ level in 12 hours of on-source integration time and a velocity resolution of 25 km s^{-1}. Lower abundance lines, such as HCN and HCO$^+$ lines, require much larger integration times at the highest angular resolution. For even high-J HCN lines at redshift 1, an on-source integration of at least 24 hr is necessary to detect the massive torus. Moreover, we predict the number count of SMGs with a massive torus (more than $10^8\ M_\odot$) of $\approx$100 deg^{-2} at redshift $1 < z < 3$. We stress the relevance of studying samples of gravitationally lensed SMGs with ALMA. Although lensing introduces the lens model problem, it can nevertheless allow a much higher spatial resolution, which can be a crucial piece of information in inferring the gas distribution and rotation law in the very central regions around the growing SMBHs. Studies of lensed and unlensed SMGs would be complementary.

It is also interesting to examine the existences of massive tori in nearby AGNs with high mass accretion rates, such as type I ULIRGs or NLS1s. From that, it is possible to reveal whether the BH growth process depends on the morphology of host galaxies and redshift. In addition, determinations of the mass ratio of massive tori and bulges in SMGs, ULIRGs, and NLS1s would verify directly the radiation-drag model. This mass ratio is basically determined by the energy conversion efficiency of nuclear fusion from hydrogen to helium, 0.007 (Umemura 2001). Finally, we should emphasize that the velocity mapping of low-z massive tori will be crucial to revealing the formation of obscuring massive tori and also the fueling process from $\sim$100 pc to $\sim$1 pc.

We wish to thank the anonymous referee for constructive suggestions and fruitful comments. We thank M. Umemura for stimulating discussions and L. Tacconi and D. Lutz for helpful insights into the topic. N. K. appreciates that M. Umemura allowed us to edit his original figure. We acknowledge financial support from the Italian MIUR and INAF.

REFERENCES

Alexander, D. M., et al. 2003, AJ, 125, 383
———. 2005a, Nature, 434, 738
———. 2005b, ApJ, 632, 736
Antonucci, R. 1993, ARA&A, 31, 473
Bahcall, J. N., et al. 1997, ApJ, 479, 642
Barvainis, R. 1987, ApJ, 320, 537
Bennett, C. L., et al. 2003, ApJS, 148, 1
Boller, Th., Brandt, W. N., & Fink, H. 1996, A&A, 305, 53
Borys, C., et al. 2005, ApJ, 635, 853
Burkert, A., & Silk, J. 2001, ApJ, 554, L151
Collin, S., & Kawaguchi, T. 2004, A&A, 426, 797
Davies, R. I., et al. 2006, ApJ, 646, 754
Djorgovski, S., Weir, N., Matthews, K., & Graham, J. R. 1991, ApJ, 372, L67
Downes, D., & Solomon, P. M. 1998, ApJ, 507, 615
———. 2003, ApJ, 582, 37
Dunlop, J. S., et al. 2003, MNRAS, 340, 1095
Duschl, W. J., Stittmatter, P. A., & Biermann, P. L. 2000, A&A, 357, 1123
Fabian, A. C., & Iwasawa, K. 1999, MNRAS, 303, L34
Ferrarese, L., Holland, F., & Walter, J. 1996, ApJ, 470, 444
Ferrarese, L., & Merritt, D. 2000, ApJ, 539, L9
Fioc, M., & Rocca-Volmerrage, B. 1997, A&A, 326, 950
Fukue, J., Umemura, M., & Mineshige, S. 1997, PASJ, 49, 673
Gao, Y., Carilli, C. L., Solomon, P. M., & Vanden Bout, P. A. 2007, ApJ, 660, L93
Gao, Y., & Solomon, P. M. 2004, ApJ, 606, 271
Granato, G. L., & Danese, L. 1994, MNRAS, 268, 235
Granato, G. L., Danese, L., & Franceschini, A. 1997, ApJ, 486, 147
Granato, G. L., et al. 2004, ApJ, 600, 580 (G04)
———. 2006, MNRAS, 368, L72
Greve, T. R., et al. 2005, MNRAS, 359, 1165
Hao, C. N., Xia, X. Y., Mao, S., Wu, H., & Deng, Z. G. 2005, ApJ, 625, 78
Hosokawa, T. 2002, ApJ, 576, 75
Imanishi, M., Nakanishi, K., & Kohno, K. 2006, AJ, 131, 2888
Jaffe, W., et al. 1993, Nature, 364, 213
Kawabe, R., Kohno, K., Ohta, K., & Carilli, C. 1999, ASP Conf. Ser. 156, Highly Redshifted Radio Lines, ed. C. L. Carilli et al. (San Francisco: ASP), 45
Kawakatu, N., Imanishi, M., & Nagao, T. 2007, ApJ, 661, 660
Kawakatu, N., & Umemura, M. 2002, MNRAS, 329, 572
Kawakatu, N., Umemura, M., & Mori, M. 2003, ApJ, 583, 85 (KUM03)
Kawakatu, N., et al. 2006, ApJ, 637, 104
Kormendy, J., & Richstone, D. 1995, ARA&A, 33, 581
Laor, A. 1998, ApJ, 505, L83
Laor, A., & Draine, B. T. 1993, ApJ, 402, 441
Lapi, A., et al. 2006, ApJ, 650, 42
Magorrian, J., et al. 1998, AJ, 115, 2285
Maiolino, R., & Rieke, G. H. 1995, ApJ, 454, 95
Maiolino, R., Ruiz, M., Rieke, G. H., & Keller, L. D. 1995, ApJ, 446, 561
Malkan, M. A., Gorjian, V., & Tam, R. 1998, ApJS, 117, 25
Marconi, A., & Hunt, L. K. 2003, ApJ, 589, L21
Marconi, A., et al. 2004, MNRAS, 351, 169
Mathur, S., Kurazkiewicz, J., & Czerny, B. 2000, MNRAS, 314, L17
McLeod, K. K., & Rieke, G. H. 1995a, ApJ, 441, 96
———. 1995b, ApJ, 454, L77
McLure, R. J., & Dunlop, J. S. 2002, MNRAS, 331, 795
———. 2001, MNRAS, 327, 199
McLure, R. J., Dunlop, J. S., & Kukula, M. J. 2000, MNRAS, 318, 693
Menéndez-Delmestre, K., et al. 2007, ApJ, 655, L65
Mineshige, S., Tsuribe, T., & Umemura, M. 1998, PASJ, 50, 233
Mineshige, S., et al. 2000, PASJ, 52, 499
Mochizuki, K., & Nakagawa, T. 2000, ApJ, 535, 118
Ohsuga, K., & Umemura, M. 2001, ApJ, 559, 157
Pounds, K. A., Done, C., & Osbore, J. P. 1995, MNRAS, 277, L5
Radford, S. J. E., Downes, D., & Solomon, P. M. 1991, ApJ, 368, L15
Richstone, D., et al. 1998, Nature, 395, A14
Salucci, P., et al. 1999, MNRAS, 307, 637
Sato, J., Umemura, M., Sawada, K., & Matsuyama, S. 2004, MNRAS, 354, 176
Shankar, F., et al. 2004, MNRAS, 354, 1020
Silva, L., et al. 2005, MNRAS, 357, 1295
Smail, I., et al. 2004, ApJ, 616, 71
Solomon, P. M., & Vanden Bout, P. A. 2005, ARA&A, 43, 677
Solomon, P. M., et al. 2003, Nature, 426, 636
Spergel, D. N., et al. 2007, ApJ, in press (astro-ph/0603449)
Suganuma, M., et al. 2006, ApJ, 639, 46
Tacconi, L., et al. 2006, ApJ, 640, 228
Tadhunter, C., Marconi, A., Axon, D., Wills, K., Robinson, T. G., & Jackson, N. 2003, MNRAS, 342, 861
Thompson, T. A., Quataert, E., & Murray, N. 2005, ApJ, 630, 167
Tielens, A. G. G. M., & Hollenbach, D. 1985, ApJ, 291, 747
Tremaine, S., et al. 2002, ApJ, 574, 740
Umemura, M. 2001, ApJ, 560, L29
Umemura, M., Fukue, J., & Mineshige, S. 1997, ApJ, 479, L97

Urry, C. M., & Padovani, P. 1995, PASP, 107, 803
Valiante, E., Lutz, D., Sturm, E., Genzel, R., Tacconi, L. J., Lehnert, M. D., & Baker, A. J. 2007, ApJ, 660, 1060
Vanden Bout, P. A., Solomon, P. M., & Maddalena, R. J. 2004, ApJ, 614, L97
van der Marel, R. P., et al. 1998, AJ, 116, 2220
Wada, K., & Norman, C. A. 2002, ApJ, 566, L21
Wada, K., & Tomisaka, K. 2005, ApJ, 619, 93
Wagg, J., et al. 2005, ApJ, 634, L13
Watabe, Y., & Umemura, M. 2005, ApJ, 618, 649
Yu, Q., & Tremaine, S. 2002, MNRAS, 335, 965